Contribution from the Laboratoire de Chimie Inorganique, CNRS URA 420, and Laboratoire de Chimie Physique des Matériaux Amorphes, CNRS URA 1104, Université de Paris-Sud, 91405 Orsay, France, Laboratoire de Chimie du Solide et Inorganique Moléculaire, CNRS URA 254, Université de Rennes I, 35042 Rennes, France, and Département de Recherches Physiques, CNRS URA 71, Université Pierre et Marie Curie, 75252 Paris, France

Spin Transition in $Fe(py)_2L(NCS)_2$ Complexes, Where py = Pyridine and L = 2,2'-Bipyrimidine (bpym) and 1,10-Phenanthroline (phen): Magnetic, Calorimetric, and Mössbauer-Effect Investigation. Crystal Structure of $[Fe(py)_2bpym(NCS)_2]\cdot 0.25py$

Renée Claude,[1a] José-Antonio Real,[1a,b] Jacqueline Zarembowitch,*[,1a] Olivier Kahn,[1a] Lahcène Ouahab,[1c] Daniel Grandjean,[1c] Kamel Boukheddaden,[1d] François Varret,[1d] and Ary Dworkin[1e]

Received January 12, 1990

The abrupt high-spin ($S = 2$) ↔ low-spin ($S = 0$) transitions in solid $[Fe(py)_2bpym(NCS)_2]\cdot 0.25py$ (**1**) and $[Fe(py)_2phen(NCS)_2]\cdot 0.5py$ (**2**) complexes (with py = pyridine, bpym = 2,2'-bipyrimidine, and phen = 1,10-phenanthroline) have been investigated by variable-temperature magnetic susceptibility, ^{57}Fe Mössbauer-effect spectrometry, and differential scanning calorimetry (DSC) measurements. The structure of the high-spin form of **1** was determined. Crystal data at 293 K: space group tetragonal $I4_1/a$, $a = 18.107$ (4) Å, $c = 29.40$ (2) Å, $Z = 16$; the noncoordinated pyridine molecules present a high thermal motion and/or a positional disorder. In the complex molecules, the pyridine rings are in trans positions and the NCS^- groups in cis positions. The transition obtained for **1** is one of the sharpest reported so far; it is centered at $T_c\downarrow \simeq 113.5$ K and $T_c\uparrow \simeq 116.5$ K. The transition presented by **2** is also abrupt, though slightly more gradual; it is centered at $T_c\downarrow \simeq T_c\uparrow \simeq 106$ K. Mössbauer and magnetic susceptibility data lead to similar thermal dependence of the high-spin molecular fraction. The Debye temperatures, evaluated from the variation of the Mössbauer total absorption as a function of temperature, provide evidence for the rearrangement of the crystal lattice upon the spin transition. The temperature dependence of ΔE_q^{HS} shows that, as expected, the ligand field is less distorted from octahedral symmetry in **1** than in **2**. The enthalpy and entropy changes associated with the spin transition are evaluated from the DSC measurements: $\Delta H = 6.5 \pm 0.5$ kJ mol^{-1} (**1**), 3.7 ± 0.5 kJ mol^{-1} (**2**); $\Delta S = 56 \pm 4$ J mol^{-1} K^{-1} (**1**), 37 ± 5 J mol^{-1} K^{-1} (**2**). The lattice vibrational contribution of the entropy variation is shown to be very weak.

Introduction

The iron(II) $S = 2$ (high-spin (HS)) ↔ $S = 0$ (low-spin (LS)) transition in complexes of the type *cis*-$FeL_2(NCS)_2$, where L is a bidentate ligand such as, for instance, 1,10-phenanthroline (phen) or 2,2'-bipyridine (bpy), has been widely investigated.[2,3] On the other hand, the studies devoted to the homologous species with general formula $Fe(py)_2L(NCS)_2$, where py = pyridine, are rare and only concern the complex $Fe(py)_2phen(NCS)_2$. However, such compounds may also exhibit a temperature-induced spin conversion. Moreover, they can be used as precursors in the elaboration of mixed-ligand systems, either of the mononuclear type $FeL'L(NCS)_2$[4] or of the binuclear type $[FeL(NCS)_2]_2L'$, according to whether L' is a bidentate or a bridging bis-bidentate ligand, respectively.

In the present paper, we report on the spin transition for the new complex $Fe(py)_2bpym(NCS)_2$ (**1**), where bpym = 2,2'-bipyrimidine, and we reexamine that of $Fe(py)_2phen(NCS)_2$ (**2**). It should be noted that, in spite of many attempts, the homologous compound $Fe(py)_2bpy(NCS)_2$, where bpy = 2,2'-bipyridine, could not be isolated in the pure state as a consequence of the very high stability of the parent compound $Fe(bpy)_2(NCS)_2$.

The synthesis of $Fe(py)_2phen(NCS)_2$ was first described in the 1960s by Spacu et al.,[5,6] the compound being characterized by its IR spectrum[6] and its iron and nitrogen chemical analysis.[5] Afterwards, these authors also reported the X-ray powder diffraction pattern and the electronic spectrum of the complex at room temperature,[7] its Mössbauer parameters at 298 and 77 K,[8] and the temperature dependence of its effective magnetic moment, which provides evidence for the existence of an abrupt spin transition at 180-185 K.[7] Recently, Herber carried out an investigation of the variable-temperature IR spectra of $Fe(py)_2phen(NCS)_2$,[9] the material used for the experiments having been prepared by a method different from that of Spacu et al. The spin transition was then observed at a critical temperature T_c of ~91 K. Such a discrepancy between the values reported for T_c led us to study this compound again.

The spin transitions presented by **1** and **2** have been investigated by using magnetic susceptibility measurements, ^{57}Fe Mössbauer spectrometry, and differential scanning calorimetry (DSC). Furthermore, the single-crystal X-ray diffraction structure of **1** was determined, and that of the high-spin starting material $Fe(py)_4(NCS)_2$ used in the syntheses was further specified.

Experimental Section

Syntheses. All the syntheses were carried out under argon, and the solvents were deoxygenated before use.

$Fe(py)_4(NCS)_2$ was prepared according to the method described by Erickson and Sutin,[10] the hydrated iron(II) perchlorate being replaced by $(NH_4)_2Fe(SO_4)_2\cdot 6H_2O$. Large yellow acicular single crystals were obtained by slowly evaporating a pyridine/acetone (in 1:2 proportion) solution of the complex. Anal. Calcd for $C_{22}H_{20}N_6S_2Fe$: C, 54.11; H, 4.10; N, 17.22; S, 13.12. Found: C, 54.01; H, 4.22; N, 17.19; S, 12.90.

$Fe(py)_2bpym(NCS)_2$ (**1**) was synthesized as follows. A 1.25-mmol sample of $Fe(py)_4(NCS)_2$ was dissolved in 6 mL of pyridine at 100 °C, and 2.50 mmol of bpym dissolved in 5 mL of pyridine was then added. Compound **1** immediately precipitated as a dark violet microcrystalline powder, which was isolated and dried under argon. From slow evaporation of the filtrate, well-shaped single crystals of **1** were obtained. Anal. Calcd for $[Fe(py)_2bpym(NCS)_2]\cdot 0.25py$, viz. $C_{21.25}H_{17.25}N_{8.25}S_2Fe$: C, 50.22; H, 3.42; N, 22.74; S, 12.62. Found: C, 49.75; H, 3.22; N, 22.32; S, 12.40.

$Fe(py)_2phen(NCS)_2$ (**2**) was prepared as follows. A 1-mmol sample of 1,10-phenanthroline in 10 mL of pyridine was added to a solution obtained by dissolving 1 mmol of $Fe(py)_4(NCS)_2$ in 100 mL of pyridine at 100 °C. The violet precipitate that formed was separated from the mixture by filtration. The red filtrate was then slowly cooled. Red-violet crystals of **2** were collected after 3 weeks and dried under an argon stream. Anal. Calcd for $[Fe(py)_2phen(NCS)_2]\cdot 0.5py$, viz. $C_{26.5}H_{20.5}N_{6.5}S_2Fe$: C, 57.89; H, 3.73; N, 16.57; S, 11.65. Found: C, 57.93; H, 3.66; N, 15.51; S, 11.60.

It should be noted that compounds **1** and **2** cannot be merely characterized by their elemental analysis. Indeed, the synthesis processes described above can possibly lead to the coexistence of equal amounts of

(1) (a) Laboratoire de Chimie Inorganique, Université de Paris-Sud. (b) Permanent address: Departamento de Quimica Inorganica, Universidad de Valencia, Valencia, Spain. (c) Université de Rennes I. (d) Université Pierre et Marie Curie. (e) Laboratoire de Chimie Physique des Matériaux Amorphes, Université de Paris-Sud.
(2) Gütlich, P. *Struct. Bonding (Berlin)* **1981**, *44*, 83.
(3) König, E.; Ritter, G.; Kulshreshtha, S. K. *Chem. Rev.* **1985**, *85*, 219.
(4) Inoue, H.; Nakajima, H.; Takahashi, T.; Uchida, H.; Shirai, T.; Fluck, E. *Bull. Chem. Soc. Jpn.* **1986**, *59*, 3483.
(5) Spacu, P.; Teodorescu, M.; Lepadatu, C. *Rev. Roum. Chim.* **1964**, *9*, 39.
(6) Spacu, P.; Teodorescu, M.; Ciomârtan D. *Rev. Roum. Chim.* **1967**, *12*, 145.
(7) Spacu, P.; Teodorescu, M.; Ciomârtan, D. *Monatsh. Chem.* **1972**, *103*, 1.
(8) Spacu, P.; Teodorescu, M.; Filotti, G.; Telnic, P. *Z. Anorg. Allg. Chem.* **1972**, *392*, 88.
(9) Herber, R. H. *Inorg. Chem.* **1987**, *26*, 173.
(10) Erickson, N. E.; Sutin, N. *Inorg. Chem.* **1966**, *5*, 1834.

0020-1669/90/1329-4442$02.50/0

Table I. Crystallographic Data for $Fe(py)_4(NCS)_2$

chem formula: $C_{22}H_{20}N_6S_2Fe$	space group: $C2/c$
fw: 488.42	λ = 0.71073 Å
a = 12.419 (3) Å	ρ_{calcd} = 1.38 g cm^{-3}
b = 13.060 (3) Å	μ(Mo Kα) = 8.31 cm^{-1}
c = 15.184 (4) Å	transm coeff = 0.72–1.27
β = 107.31°	$R(F_o)$ = 0.025
V = 2351.2 Å^3	$R_w(F_o)$ = 0.036
Z = 4	
T = 25 °C	

Table II. Crystallographic Data for $[Fe(py)_2bpym(NCS)_2]\cdot 0.25py$

chem formula: $C_{21.25}H_{17.25}N_{8.25}S_2Fe$	space group: $I4_1/a$
fw: 508.16	λ = 0.71073 Å
a = 18.107 (4) Å	ρ_{calcd} = 1.401 g cm^{-3}
c = 29.40 (2) Å	μ(Mo Kα) = 8.16 cm^{-1}
V = 9638 Å^3	transm coeff = 0.72–1.27
Z = 16	$R(F_o)$ = 0.064
T = 25 °C	$R_w(F_o)$ = 0.065

a complex $FeL_2(NCS)_2$ and of the remaining precursor $Fe(py)_4(NCS)_2$, which would result in the same elemental analysis as that of the expected compound. For both syntheses, the absence of $FeL_2(NCS)_2$ and $Fe(py)_4(NCS)_2$ complexes in the final product was clearly demonstrated from infrared spectra.

X-ray Crystallographic Analysis. X-ray diffraction measurements were performed on an Enraf-Nonius CAD-4 diffractometer with graphite-monochromated Mo Kα radiation.

The crystal structure of $Fe(py)_4(NCS)_2$ has been already described.[11] However, owing to the rather low accuracy of the data (R being found as 6.35%, to be compared with 2.5% in the present study (vide infra)) and to the possible existence of several forms for the compound,[6,11] we decided to reinvestigate it. Intensity data were recorded at room temperature. Details on crystal characteristics, data collection, and structure refinement are reported in Table I. All the other results concerning this structure, except the most significant bond lengths and angles, which will be given hereafter, are presented as supplementary material.

The structure of **1** was solved by using room-temperature data. Crystal and refinement data are summarized in Table II. Lattice parameters were determined and refined by the least-squares method from 25 centered reflections. The intensities were collected by the θ–2θ scan mode and corrected for Lorentz and polarization effects. On the basis of the systematic absences (hkl, $h + k + l = 2n + 1$; $hk0$, $h = 2n + 1$; $00l$, $l = 4n + 1$), the tests $I_{hkl} \neq I_{khl}$, and the successful solution and refinement of the structure, the space group was determined to be $I4_1/a$. Data collections were performed on crystals issued from different preparations.

The structure was solved by direct methods[12] and successive Fourier differences. In the final refinement, the non-hydrogen atoms were treated anisotropically, and all hydrogen atoms were idealized and updated (C–H = 1.0 Å, B_{eq} = 4 Å^2). The large thermal coefficients obtained for the atoms of the noncoordinated pyridine molecule revealed high thermal motion and/or positional disorder, so that unambiguous identification of the nitrogen atom was not possible; the atoms of this solvent molecule were then refined isotropically with a multiplicity fixed at 0.25 on the basis of the microanalysis data. The SDP computing programs described by Frenz[13] were used. Atomic scattering factors were taken from ref 14. The atomic coordinates and isotropic thermal parameters for the most significant non-hydrogen atoms are given in Table III.

Magnetic Measurements. The temperature dependence of the magnetic susceptibility was determined, for compounds **1** and **2**, with a Faraday-type magnetometer equipped with an Oxford Instruments helium continuous-flow cryostat. The independence of the susceptibility with regard to the applied magnetic field was checked for each compound at room temperature. Mercury tetrakis(thiocyanato)cobaltate was used as a susceptibility standard. Diamagnetic corrections were estimated to be -260×10^{-6} cm^3 mol^{-1} for **1** and -360×10^{-6} cm^3 mol^{-1} for **2**. Temperature was varied at the rate of 1 K min^{-1} in the cooling mode and ~0.5 K min^{-1} in the heating mode.

Table III. Positional Parameters and Equivalent B's and Their Estimated Standard Deviations for the Most Significant Non-H Atoms of $[Fe(py)_2bpym(NCS)_2]\cdot 0.25py$ (**1**) at T = 293 K

	x	y	z	B_{eq}, Å^2
Fe	0.22188 (8)	0.02160 (8)	0.09095 (5)	3.68 (3)
S(1)	0.3950 (2)	0.2207 (2)	0.0778 (2)	8.0 (1)
S(2)	0.0633 (2)	0.1079 (2)	−0.0302 (1)	5.64 (8)
N(1)	0.2901 (5)	0.1164 (4)	0.0913 (3)	4.3 (2)
N(2)	0.1478 (4)	0.0432 (5)	0.0377 (3)	4.4 (2)
N(3)	0.2832 (4)	−0.0281 (4)	0.1484 (2)	3.3 (2)
N(5)	0.1759 (4)	−0.0911 (4)	0.1011 (3)	3.5 (2)
N(7)	0.3035 (4)	−0.0340 (5)	0.0449 (3)	4.3 (2)
N(8)	0.1414 (5)	0.0726 (4)	0.1389 (3)	4.2 (2)
C(1)	0.3300 (6)	0.1585 (5)	0.0849 (3)	3.7 (3)
C(2)	0.1140 (6)	0.0687 (6)	0.0104 (3)	3.8 (3)
C(3)	0.2717 (5)	−0.0999 (5)	0.1568 (3)	3.4 (2)
C(6)	0.3339 (6)	0.0088 (6)	0.1746 (4)	4.5 (3)
C(7)	0.2128 (6)	−0.1363 (5)	0.1286 (4)	4.1 (3)
C(8)	0.1234 (6)	−0.1220 (6)	0.0769 (4)	4.1 (3)
C(11)	0.2836 (6)	−0.0786 (6)	0.0114 (4)	4.6 (3)
C(15)	0.3752 (6)	−0.0275 (7)	0.0525 (4)	4.9 (3)
C(16)	0.0693 (6)	0.0554 (6)	0.1396 (4)	5.0 (3)
C(20)	0.1644 (6)	0.1235 (6)	0.1689 (4)	5.0 (3)

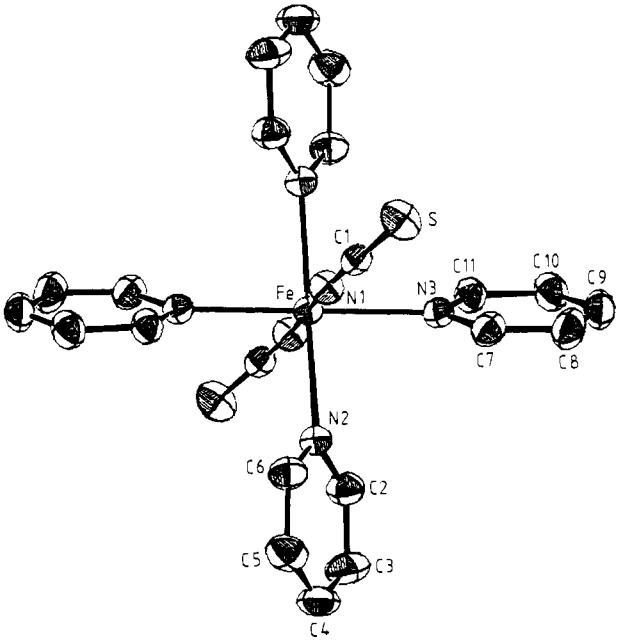

Figure 1. Perspective view of the $Fe(py)_4(NCS)_2$ molecule, showing the atom-labeling scheme.

Mössbauer Spectra. The Mössbauer spectra were recorded on a constant-acceleration spectrometer, with a 25-mCi source of ^{57}Co in rhodium matrix. The polycrystalline absorber contained 35 mg of material/cm^2, i.e. ~0.08 mg cm^{-2} of ^{57}Fe. Variable-temperature spectra, in the 295–4.2 K range, were obtained by using a standard cryostat (OXIN CD-3); temperature was controlled by a linear sensor (OXIN-CLTS) calibrated at 77 K. After folding of the spectra, the experimental width of the lines, in the considered velocity range, is Γ_{exp} = 0.215 mm s^{-1}. Least-squares-fitted parameters are given with their standard deviation of statistical origin (in parentheses); isomer shift values refer to metallic iron at room temperature. For a detailed investigation of the spin transition, the so-called "thermal scanning method" was used. This fast-counting method consists of the recording of the spectra as a function of temperature, with a constant velocity of the source chosen so as to match an absorption line of the high-spin species; the temperature was decreased or increased by steps of 1 K every 10 min, and 2 min was left before each counting.

Calorimetric Measurements. The differential scanning calorimetry analysis was conducted on a Perkin-Elmer DSC-2 instrument, the low-temperature attachment of which was either a cold finger plunging in a liquid-nitrogen bath (for **1**) or a home-made cooling system allowing the temperature to be lowered to 83 K[15] (for **2**), helium being used as the

(11) Sotofte, I.; Rasmussen, S. E. *Acta Chem. Scand.* **1967**, *21*, 2028.
(12) Main, P.; Fiske, S. J.; Hull, S. E.; Lessinger, L.; Germain, G.; Declercq, J. P.; Woolfson, M. M. MULTAN 84, A System of Computer Programs for the Automatic Solution of Crystal Structures from X-ray Diffraction Data. University of York, England, and University of Louvain, Belgium, 1984.
(13) Frenz, B. A. In *Computing in Crystallography*; Schenk, H., Olthofhazekamp, R., van Koningsveld, H., Bassi, G. C. Eds.; Delft University Press: 1978; p 64.
(14) *International Tables for X-ray Crystallography*; Kynoch Press: Birmingham, England, 1974; Vol. IV.
(15) Dworkin, A.; Szwarc, H. *High Temp.—High Pressures* **1989**, *21*, 195.

Table IV. Selected Bond Lengths (Å) and Angles (deg) for $Fe(py)_4(NCS)_2$[a]

Fe-N(1)	2.106 (3)	S-C(1)	1.627 (3)
Fe-N(2)	2.241 (2)	N(1)-C(1)	1.135 (4)
Fe-N(3)	2.260 (2)		
N(1)-Fe-N(2)	89.06 (9)	Fe-N(2)-C(6)	122.2 (2)
N(1)-Fe-N(3)	89.35 (9)	Fe-N(3)-C(7)	121.5 (2)
N(2)-Fe-N(3)	92.87 (8)	Fe-N(3)-C(11)	121.2 (2)
Fe-N(1)-C(1)	155.9 (2)	S-C(1)-N(1)	179.2 (3)
Fe-N(2)-C(2)	121.4 (2)		

[a] Numbers in parentheses are estimated standard deviations in the least significant digits.

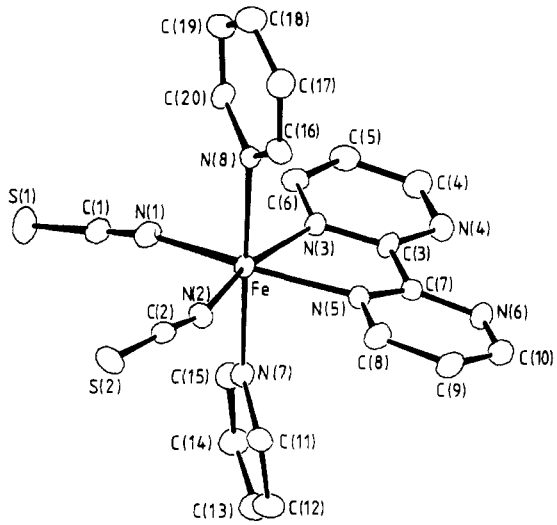

Figure 2. Perspective view of the $Fe(py)_2bpym(NCS)_2$ molecule, showing the atom-labeling scheme.

purge gas. Sealed sample pans were employed. Cooling as well as heating curves were recorded and analyzed with the TADS-3600 Perkin-Elmer system. Temperature and enthalpy were calibrated with a sample of pure cyclohexane by using its melting (279.69 K, 2678 J mol^{-1}) and crystal-to-crystal transitions (186.10 K, 6740 J mol^{-1}). The temperature values are given with a ±0.5 K accuracy, and the enthalpies are determined with an experimental uncertainty of ±2% for a scan rate of 10 K min^{-1}.

Results

Description of the Structures. Structure of $Fe(py)_4(NCS)_2$. A perspective view of the molecule is shown in Figure 1. Bond lengths and angles are given in Table IV. The iron(II) ion is located on a crystallographic inversion center and is surrounded by six nitrogen atoms belonging to two thiocyanate groups in the trans position and four pyridine molecules. The Fe-N bond lengths involving NCS^- (Fe-N(1) = 2.106 (3) Å) are shorter than those involving the pyridine ligands (Fe-N(2) = 2.241 (2) Å, Fe-N(3) = 2.260 (2) Å). As already observed,[11] the Fe-N(1)-C(1) angle strongly deviates from 180°. It is actually found to be 155.9 (2)°.

Structure of $[Fe(py)_2bpym(NCS)_2]$·0.25py. A perspective view of the molecule is shown in Figure 2, and the projection of the unit cell along the *b* axis, in Figure 3. The most significant bond lengths and angles are given in Table V. The iron(II) ion is surrounded by six nitrogen atoms belonging to two thiocyanate groups in the cis position, two pyridine molecules in the trans position, and a bipyrimidine molecule. As for $Fe(py)_4(NCS)_2$, the Fe-N bond lengths involving NCS^- (Fe-N(1) = 2.115 (8) Å, Fe-N(2) = 2.098 (8) Å) are much shorter than those involving the N-heterocycle ligands (from 2.212 (7) to 2.224 (8) Å), which leads to a pronounced distortion of the FeN_6 octahedron. Furthermore, whereas the N-C-S groups are quasi-linear, the Fe-N-C(S) linkages are significantly bent (Fe-N(1)-C(1) = 167.1 (9)°, Fe-N(2)-C(2) = 165.9 (9)°).

Magnetic Susceptibility Data. The magnetic properties of **1** and **2** are presented in Figures 4 and 5, in the form of $\chi_M T$ vs T plots, χ_M being the molar magnetic susceptibility and T the temperature. The data were recorded in both the cooling and warming modes in order to detect a possible hysteresis effect.

For **1**, $\chi_M T$ is equal to 3.40 cm^3 mol^{-1} K (which corresponds to an effective magnetic moment of 5.22 μ_B) at room temperature and remains almost constant upon cooling to ~150 K. Thereafter, it decreases slowly between ~150 and 114 K and very abruptly between 114 and 113 K. About 75% of the transition occurs within 1 K. Upon further cooling, $\chi_M T$ tends toward a residual value of 0.15 cm^3 mol^{-1} K (μ_{eff} = 1.10 μ_B), which indicates the presence of ~4% of paramagnetic high-spin species in the low-spin matrix. As the temperature increases, the transition is again very abrupt but occurs between 116 and 117 K. A hysteresis of ca. 3 K is therefore observed.

For **2**, the critical temperature of the transition is $T_c \simeq 106$ K, in both the heating and the cooling modes. The hysteresis

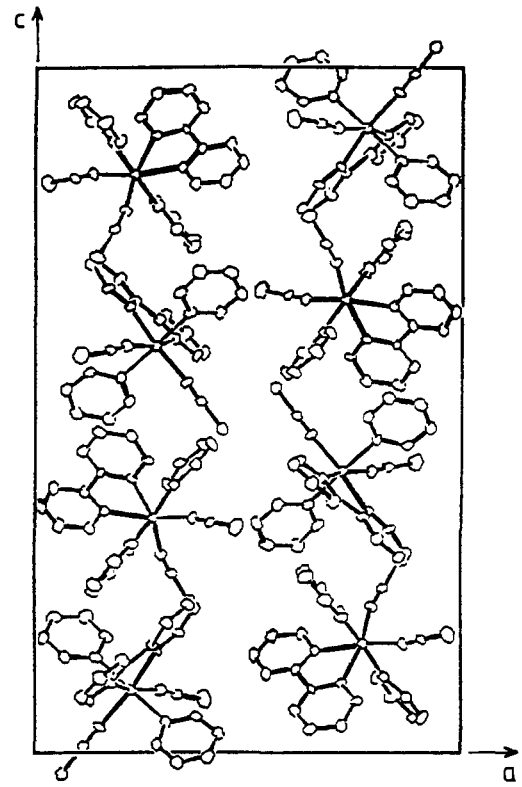

Figure 3. Projection of the crystal structure of $[Fe(py)_2bpym(NCS)_2]$·0.25py along the *b* axis. For clarity, the pyridine solvent molecules have been omitted.

Table V. Selected Bond Lengths (Å) and Angles (deg) for $[Fe(py)_2bpym(NCS)_2]$·0.25py[a]

Fe-N(1)	2.115 (8)	Fe-N(8)	2.228 (8)
Fe-N(2)	2.098 (8)	S(1)-C(1)	1.641 (11)
Fe-N(3)	2.212 (7)	S(2)-C(2)	1.664 (10)
Fe-N(5)	2.224 (8)	N(1)-C(1)	1.067 (13)
Fe-N(7)	2.242 (8)	N(2)-C(2)	1.110 (13)
N(1)-Fe-N(2)	103.0 (3)	Fe-N(1)-C(1)	167.1 (9)
N(1)-Fe-N(3)	91.9 (3)	Fe-N(2)-C(2)	165.9 (9)
N(1)-Fe-N(5)	164.3 (3)	Fe-N(3)-C(3)	117.2 (6)
N(1)-Fe-N(7)	89.0 (3)	Fe-N(3)-C(6)	124.6 (6)
N(1)-Fe-N(8)	92.4 (3)	Fe-N(5)-C(7)	117.3 (6)
N(2)-Fe-N(3)	165.1 (3)	Fe-N(5)-C(8)	126.1 (7)
N(2)-Fe-N(5)	91.8 (3)	Fe-N(7)-C(11)	122.9 (7)
N(2)-Fe-N(7)	93.1 (3)	Fe-N(7)-C(15)	120.3 (7)
N(2)-Fe-N(8)	88.7 (3)	Fe-N(8)-C(16)	123.3 (7)
N(3)-Fe-N(5)	73.3 (3)	Fe-N(8)-C(20)	119.9 (7)
N(3)-Fe-N(7)	87.0 (3)	S(1)-C(1)-N(1)	176. (1)
N(3)-Fe-N(8)	90.8 (3)	S(2)-C(2)-N(2)	179. (1)
N(5)-Fe-N(7)	85.1 (3)	N(3)-C(3)-C(7)	115.8 (8)
N(5)-Fe-N(8)	92.9 (3)	N(5)-C(7)-C(3)	114.9 (8)
N(7)-Fe-N(8)	177.4 (3)		

[a] Numbers in parentheses are estimated standard deviations in the least significant digits.

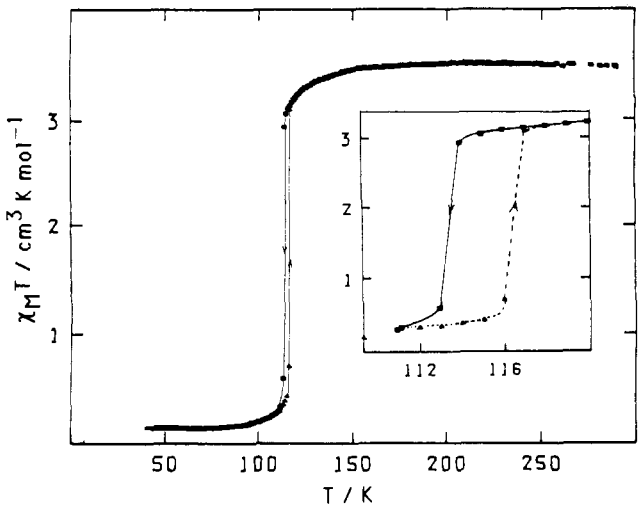

Figure 4. Temperature dependence of $\chi_M T$ for compound **1**. Falling and rising arrows indicate decreasing and increasing temperatures, respectively. $T_c\downarrow \simeq 113.5$ K; $T_c\uparrow \simeq 116.5$ K. Higher plateau: $\chi_M T = 3.40$ cm^3 mol^{-1} K ($\mu_{eff} = 5.22\ \mu_B$). Lower plateau: $\chi_M T = 0.15$ cm^3 mol^{-1} K ($\mu_{eff} = 1.10\ \mu_B$).

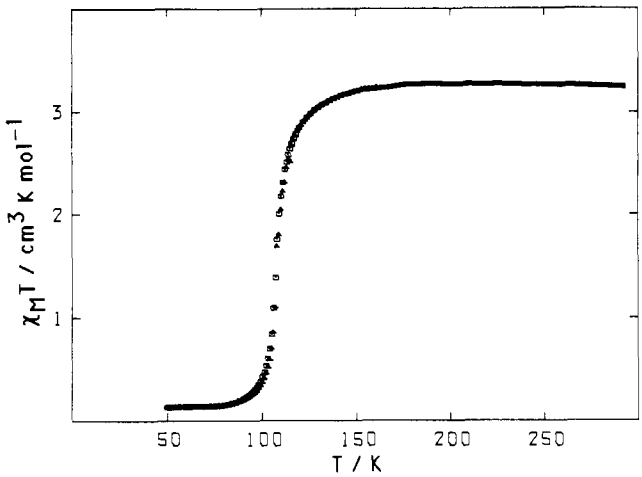

Figure 5. Temperature dependence of $\chi_M T$ for compound **2**, in the cooling (□) and heating (▲) modes. $T_c\downarrow \simeq T_c\uparrow \simeq 106$ K. Higher plateau: $\chi_M T = 3.27$ cm^3 mol^{-1} K ($\mu_{eff} = 5.11\ \mu_B$). Lower plateau: $\chi_M T = 0.14$ cm^3 mol^{-1} K ($\mu_{eff} = 1.06\ \mu_B$).

effect, if present, is lower than 0.5 K. The transition is significantly less abrupt than for **1**: 75% of the spin conversion occurs within ca. 16 K. The upper and lower plateaus of the $\chi_M T$ vs T plot correspond to $\chi_M T = 3.27$ and 0.14 cm^3 mol^{-1} K ($\mu_{eff} = 5.11$ and 1.06 μ_B), respectively. The latter value provides evidence for the existence of a residual amount of high-spin molecules in the predominant low-spin isomer at low temperatures. As in **1**, this amount can be estimated as ~4%.

Mössbauer Spectrometry Data. The temperature dependence of the ^{57}Fe Mössbauer spectra has been studied, for both $Fe(py)_2L(NCS)_2$ absorbers, between room temperature and 4.2 K.

Figures 6 and 7 show a selection of some representative spectra obtained at increasing temperatures for **1** and **2**, respectively. The dominant doublet observed at 290 (**1**) and 298 K (**2**) is characterized by the quadrupole splitting $\Delta E_q = 1.640$ (4) (**1**) and 2.010 (1) mm s^{-1} (**2**) and the isomer shift IS = +1.001 (2) (**1**) and +1.005 (1) mm s^{-1} (**2**). It corresponds to the $S = 2$ high-spin ground state of iron(II). As the temperature is lowered, another doublet appears (between the two previous peaks), the intensity of which increases at the expense of that of the first one. Its characteristics at 4.2 K are $\Delta E_q = 0.484$ (2) (**1**) and 0.401 (1) mm s^{-1} (**2**) and IS = +0.469 (1) (**1**) and +0.472 (1) mm s^{-1} (**2**). They are typical of the $S = 0$ low-spin ground state of iron(II). It should be noted that **1** undergoes a decomposition in the solid state. The additional weak doublet observed in each spectrum of this compound (see for instance the spectra obtained at 290 and 4.2 K, in Figure 6) is attributed to the presence of a small amount of the iron derivative resulting from that decomposition. The relevant Mössbauer parameters were found to be consistent with those determined for the binuclear species $[Fe(bpym)(NCS)_2]_2bpym$, which is not surprising since this complex was reported to be a very stable HS species.[16]

Detailed values of the Mössbauer parameters for **1** and **2**, including the area ratio A_{HS}/A_{tot} (A being the base-line-corrected area), are listed in Table VI for a representative set of temperatures.

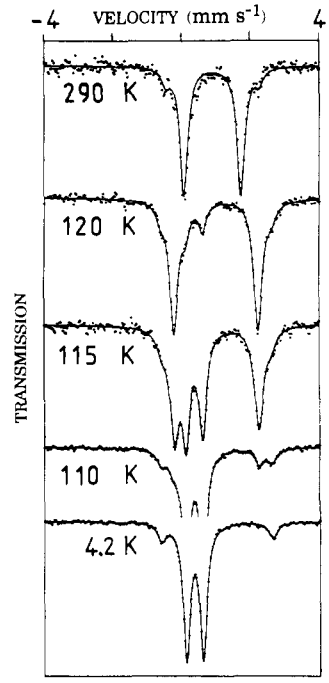

Figure 6. ^{57}Fe Mössbauer spectra of **1** for a representative set of temperatures. Measurements were performed in the heating mode. The outer weak doublet results from the presence of a small amount of impurity (see the text).

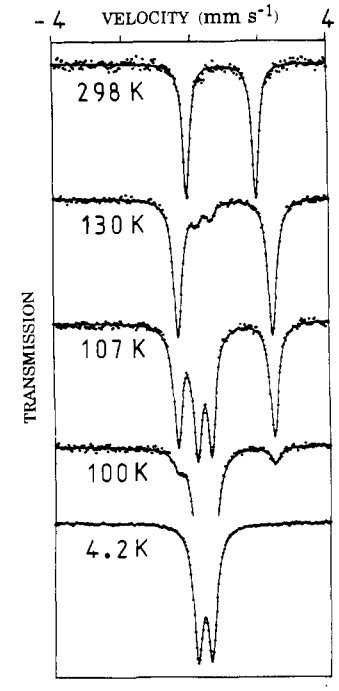

Figure 7. ^{57}Fe Mössbauer spectra of **2** for a representative set of temperatures. Measurements were performed in the heating mode.

(16) Real, J. A.; Zarembowitch, J.; Kahn, O.; Solans, X. *Inorg. Chem.* **1987**, *26*, 2939.

Table VI. ^{57}Fe Mössbauer-Effect Parameters[a] of $[Fe(py)_2bpym(NCS)_2]\cdot 0.25py$ (**1**) and $[Fe(py)_2phen(NCS)_2]\cdot 0.5py$ (**2**) for a Set of Representative Temperatures[b]

T, K	IS^{LS}, mm s^{-1}	ΔE_q^{LS}, mm s^{-1}	IS^{HS}, mm s^{-1}	ΔE_q^{HS}, mm s^{-1}	$10^2 A_{HS}/A_{tot}$[c]
		Compound **1**			
4.2	0.469 (1)	0.482 (2)			0
78	0.471 (1)	0.491 (1)			0
100	0.470 (1)	0.492 (1)	1.109 (5)	2.470 (2)	7 (2)
110	0.468 (1)	0.490 (1)	1.115 (4)	2.460 (1)	14 (2)
115	0.470 (2)	0.480 (4)	1.114 (2)	2.431 (4)	48 (2)
120	0.470 (2)	0.480 (4)	1.104 (1)	2.419 (3)	83 (2)
200			1.066 (1)	2.042 (2)	100
290			1.001 (2)	1.640 (4)	100
		Compound **2**			
4.2	0.472 (1)	0.401 (1)			0
78	0.464 (1)	0.406 (1)			0
100	0.471 (1)	0.409 (2)	1.110 (7)	2.810 (1)	12 (2)
107	0.467 (1)	0.410 (2)	1.099 (1)	2.788 (3)	49 (2)
120	0.460 (1)	0.395 (8)	1.092 (1)	2.757 (2)	83 (2)
200			1.062 (2)	2.462 (4)	100
298			1.005 (1)	2.010 (2)	100

[a] Isomer shifts are referred to metallic iron at room temperature. [b] The values listed were obtained for rising temperatures. [c] A: area of the lines. In the case of **1**, the values of A_{HS}/A_{tot} have been corrected for the presence of a small amount of decomposition product in the sample (see the text).

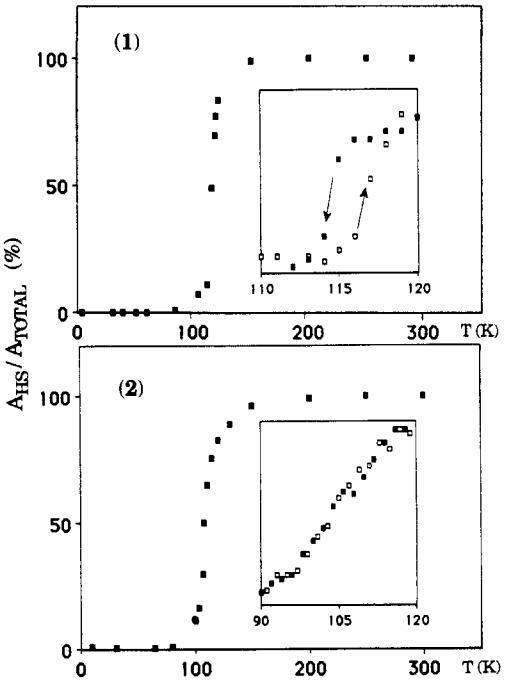

Figure 8. Temperature dependence of the area ratio A_{HS}/A_{tot} for **1** and **2**, derived from Mössbauer-effect measurements performed in the heating mode. The insets represent thermal scannings of the high-spin lines (cf. the Experimental Section), carried out for decreasing (■) and increasing (□) temperatures at the rate of ca. 1 K every 10 min (the ordinates are in arbitrary units).

Plots of A_{HS}/A_{tot} as a function of temperature are given in Figure 8. For thin absorbers, such as those used in that work, the total area of the spectra can be expressed as[17]

$$A_{tot} = C(f_{HS}n_{HS} + f_{LS}n_{LS}) \quad (1)$$

C being a constant that partly depends on the sample, f_{HS} and f_{LS} the Lamb–Mössbauer factors of the high- and low-spin forms, n_{HS} and $n_{LS} = 1 - n_{HS}$ the respective fractions of these forms. Assuming, to a first approximation (as will be detailed further), that $f_{HS} \approx f_{LS}$, it follows that

$$A_{HS}/A_{tot} \approx n_{HS} \quad (2)$$

(17) König, E.; Ritter, G.; Goodwin, H. A. *Chem. Phys.* **1973**, *1*, 17.

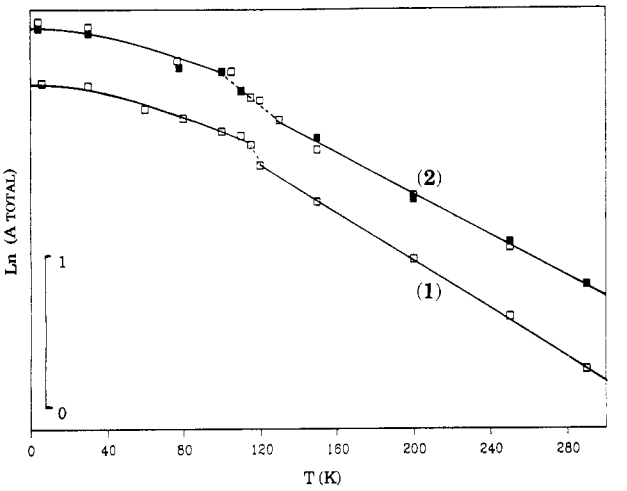

Figure 9. Temperature dependence of ln A_{tot} for **1** and **2**, derived from measurements carried out in the heating mode. For **2**, □ and ■ are relative to two different samples. For clarity, the curves were separated from each other by a translation along the ordinate axis. Full lines represent fitted curves. Dotted lines were added to point out the spin-crossover region.

So, the curves A_{HS}/A_{tot} vs T qualitatively represent the thermal behavior of the high-spin fraction, but the difference in the Lamb–Mössbauer factors of the two spin isomers is not taken into account. In the present case, this difference is expected to be rather small due to the relatively low transition temperatures. The transition is found to be centered at $T_c\uparrow$ = 116–117 K for **1** and $T_c\uparrow$ = 106–107 K for **2**. Thermal scannings of the high-spin lines, performed both in the cooling and the warming modes in the temperature range of the transition, led to the values $T_c\downarrow \simeq$ 114.5 K and $T_c\uparrow \simeq$ 116.7 K for **1** and $T_c\downarrow \simeq T_c\uparrow \simeq$ 106 K for **2** (see the insets in Figure 8). Thus, evidence seems again provided for the existence of a thermal hysteresis (found here to be ca. 2.2 K) for **1** and the absence of a noticeable hysteresis for **2**.

The temperature dependence of ln A_{tot}, derived from measurements carried out in the heating mode, is displayed in Figure 9 for compounds **1** and **2**. In both cases, the spin transition results in an appreciable discontinuity of the slope. In the temperature range where only the high-spin species exists, the curves are linear. This shows, since the area A_{HS} is then proportional to the recoil-free fraction f_{HS} (see eq 1, with $n_{HS} = 1$), that the variation of f_{HS} as a function of temperature does obey the high-temperature approximation of the Debye model[18,19]

$$\ln f_{T \geq \Theta_D/2} = \frac{-3E_0^2}{Mc^2k_B}\left(\frac{T}{\Theta_D^2}\right) \quad (3)$$

Here, Θ_D is the Debye temperature, E_0 the γ-ray energy, and M the effective mass of the absorbing atom, c and k_B having their usual meaning; hence $3E_0^2/Mc^2k_B$ = 136 K, when M is taken as the mass of the iron atom, viz. 57 amu. The Θ_D values, estimated for high-spin phases from the slopes of the two straight lines, are found to be Θ_D^{HS} = 132 ± 1 K for **1** and 140 ± 2 K for **2**.

In the low-temperature range, where the systems are in their low-spin form, the curves are no longer linear. In that case, a realistic analysis of the data requires the use of the actual thermal dependence of f in the Debye model

$$\ln f = \frac{-3E_0^2}{2Mc^2k_B}\left[1 + \left(\frac{T}{\Theta_D}\right)^2 \int_0^{\Theta_D/T} \frac{x\,dx}{e^x - 1}\right] \quad (4)$$

Thickness corrections are also needed, since they become sizable at low temperatures. They were accounted for by a simplified procedure recently described.[20] The experimental data of ln A_{tot}

(18) Janot, C. *L'Effet Mössbauer et ses Applications*; Collection de Monographies de Physique; Masson & Cie: Paris, 1972; Vol. 8.
(19) Parish, R. V. In *Mössbauer Spectroscopy Applied to Inorganic Chemistry*; Long, G. J., Ed.; Plenum: New York, 1984; Vol. 1, p 527.

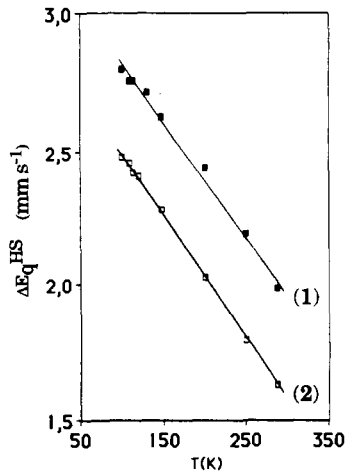

Figure 10. Temperature dependence of the quadrupole splitting, ΔE_q^{HS}, for the high-spin forms of **1** and **2**. Straight lines were drawn to point out the quasi-linearity of the variation.

as a function of T were analyzed by fitting the scaling parameter C of eq 1, Θ_D^{LS}, and $\Delta\Theta_D = \Theta_D^{LS} - \Theta_D^{HS}$. The full lines drawn in Figure 9 were obtained with the following values: $\Theta_D^{LS} = 149$ (5) K and $\Delta\Theta_D = 16$ (4) K for **1** and $\Theta_D^{LS} = 148$ (7) K and $\Delta\Theta_D = 13$ (5) K for **2**. These results are consistent with the Θ_D^{HS} values obtained in the high-temperature approach.

It is worth noting that the Θ_D values quoted above are certainly overestimated, owing to the presence of covalent bonds which increases the effective mass of the iron atom. However, they are meaningful for comparing **1** and **2** and give upper limits for $\Delta\Theta_D$ values. Also, as assumed when introducing eq 2, it is confirmed that the f factors vary relatively little at the transition ($|\Delta f/f_{LS}| \approx 18\%$ for **1** and $\approx 13\%$ for **2**).

Finally, the variations of ΔE_q^{HS} as a function of temperature are represented in Figure 10 for both complexes.

Thermodynamic Parameters. Typical sets of DSC curves, recorded for a heating and cooling rate of 10 K min^{-1}, are shown in Figure 11.

The peaks obtained for increasing temperatures show that the transition process is then endothermic, its onset being found at 116.0 (**1**) and 100.1 K (**2**). The exothermic peaks that form in the cooling mode lead to the onset values of 109.2 (**1**) and 104.7 K (**2**). The average values of the enthalpy change, obtained for a number of experiments carried out at increasing and decreasing temperatures, are found to be $\Delta H = 6.5 \pm 0.5$ (**1**) and 3.7 ± 0.5 kJ mol^{-1} (**2**) after correction for the presence of high-spin impurity and/or residual high-spin isomer at low temperature. The derived values of the entropy change, calculated with the onset temperatures determined in the heating mode, are $\Delta S = 56 \pm 4$ (**1**) and 37 ± 5 J mol^{-1} K^{-1} (**2**).

Discussion

The first point we wish to emphasize in this discussion concerns the molecular rearrangement accompying the reaction

$$Fe(py)_4(NCS)_2 + bpym \rightarrow Fe(py)_2bpym(NCS)_2 + 2py$$

In the starting compound the two NCS^- groups are in the trans position, whereas in the final compound they are in the cis position. It should be noted that, when such groups behave as ligands in Fe(II) pseudooctahedral spin-crossover complexes, they are generally cis oriented. Only one exception is currently known: in $[Fe(4,4'\text{-bi-}1,2,4\text{-triazole})_2(NCS)]\cdot H_2O$ the thiocyanate groups are trans oriented.[21]

The values obtained for the main structural parameters of $[Fe(py)_2bpym(NCS)_2]\cdot 0.25py$, in particular Fe–N(bpym) distances (2.224 (8) and 2.212 (7) Å), Fe–N(CS) distances (2.098 (8) and 2.115 (8) Å), and Fe–N–C(S) angles (165.9 (9) and 167.1 (9)°), are found to be close to the homologous values reported for the spin-crossover complexes $Fe(phen)_2(NCS)_2$,[22] $Fe(bpy)_2(NCS)_2$,[23] and $Fe(btz)_2(NCS)_2$[24] (btz = 2,2'-bi-4,5-dihydrothiazine) and for the parent binuclear species $[Fe(bpym)(NCS)_2]_2bpym$.[16] In these compounds, the average distances of Fe–N(heterocycle) bonds range from 2.17 to 2.22 Å, those for Fe–N(CS) bonds vary from 2.05 to 2.09 Å, and the mean value of Fe–N–C(S) angles varies from 160.1 to 170.7°. However, the most striking feature in the structure of **1** is the disorder presented by the noncoordinated pyridine. Such a solvent molecule disorder has been previously pointed out in the high-spin form of some spin-crossover complexes[25] as $[Fe^{II}(2\text{-pic})_3]Cl_2\cdot C_2H_5OH$, $[Fe^{II}(dppen)_2Cl_2]\cdot((CH_3)_2CO)_2$, and $[Fe^{III}(C_4H_8ONC(S)S)_3]\cdot CH_2Cl_2$ (with 2-pic = 2-picolylamine, dppen = *cis*-1,2-bis(diphenylphosphino)ethylene, $C_4H_8ONC(S)S$ = 4-morpholinecarbodithioate). For these compounds, the spin conversion was shown to be accompanied by an order–disorder transition of the solvent molecules.

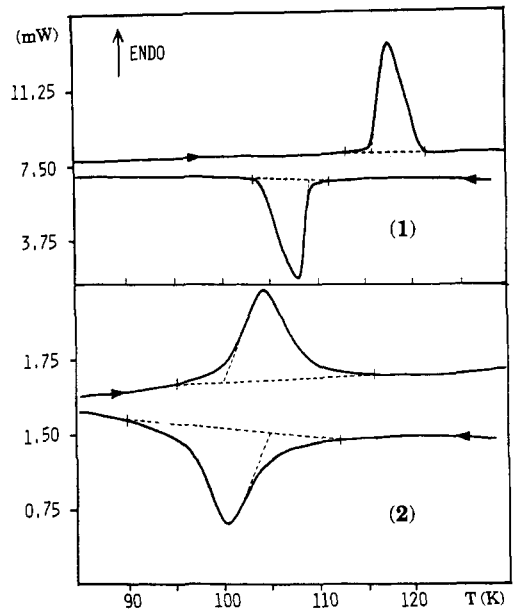

Figure 11. DSC curves obtained for **1** and **2** at a scan rate of 10 K min^{-1}.

As for compound **2**, the nearly complete and rather sharp spin transition observed around 106 K is quite different from the transition reported by Spacu et al. for $Fe(py)_2phen(NCS)_2$ from magnetic susceptibility measurements.[7] Indeed, the latter occurs at a temperature of 180–185 K, and on cooling, the effective magnetic moment tends toward a lower limit of $\sim 2\ \mu_B$ ($\chi_M T \sim 0.5$ cm^3 mol^{-1} K), which corresponds to the presence of $\sim 15\%$ of high-spin species in the low-spin isomer.

These data and a close comparison of the infrared spectra[6,7] and Mössbauer parameters[8] reported by Spacu et al. with those obtained for **2** (present work), $Fe(py)_4(NCS)_2$,[26] and $Fe(phen)_2(NCS)_2$[27,28] clearly show that the samples examined by these authors were chiefly constituted by $Fe(phen)_2(NCS)_2$ (which exhibits a spin transition at ~ 176 K), the other components being variable amounts of $Fe(py)_4(NCS)_2$ and/or $Fe(py)_2phen(NCS)_2$. The main characteristics of the infrared spectrum of **2** are a rather well-defined doublet at 2027 and 2038 cm^{-1}, corresponding to ν(C–N(CS)) stretching modes, and the presence of two separated intense bands in the range 680–735 cm^{-1}, at 698 (very strong)

(20) Boukheddaden, K.; Varret, F. Submitted for publication in *Hyperfine Interact.*
(21) Vreugdenhil, W.; van Diemen, J.; de Graaff, R. A. G.; Haasnoot, J. G.; van der Kraan, A. M.; Kahn, O.; Zarembowitch, J.; Reedijk, J. Submitted for publication in *Polyhedron.*
(22) Gallois, B.; Real, J. A.; Hauw, C.; Zarembowitch, J. *Inorg. Chem.* **1990**, *29*, 1152.
(23) König, E.; Watson, K. J. *Chem. Phys. Lett.* **1970**, *6*, 457.
(24) Real, J. A.; Gallois, B.; Granier, T.; Suez-Panama, F.; Zarembowitch, J. To be published.
(25) König, K. *Prog. Inorg. Chem.* **1987**, *35*, 527.
(26) Bousseksou, A.; Varret, F.; Claude, R. To be published.
(27) Ganguli, P.; Gütlich, P.; Müller, E. W. *J. Chem. Soc., Dalton Trans.* **1981**, 441.
(28) König, E.; Madeja, K. *Spectrochim. Acta* **1967**, *23A*, 45.

and 727 cm^{-1} (strong). The slight discrepancy between the critical transition temperature we obtained for **2** and that reported by Herber[9] from variable-temperature Fourier transform infrared spectra (~91 K) might arise from the fact that our compound was a pyridine solvate, contrary to that examined by Herber.

Let us now examine the Mössbauer spectrometry data. The plots of A_{HS}/A_{tot} vs T (cf. Figure 8) are quite similar to those of $\chi_M T$ vs T (cf. Figures 4 and 5). This is not surprising since $\chi_M T$ is proportional to the high-spin fraction n_{HS} and the same holds for A_{HS}/A_{tot} (see eq 2) within the approximation $f_{HS} \approx f_{LS}$ (which is thus justified). The derived transition critical temperatures are found to be in agreement. The small amount of residual HS form at low temperatures (~4%), observed for both compounds from magnetic susceptibility measurements, is not evidenced from Mössbauer spectra. This is likely to result from slight differences between the samples examined. Those used for magnetism experiments might exhibit a higher density of crystal imperfections and/or a slightly larger amount of HS impurities (e.g. decomposition product (for **1**), starting material $Fe(py)_4(NCS)_2$) than those used for Mössbauer experiments.

The analysis of the Debye temperatures gives some insight into the low-frequency vibrational modes. For both compounds, the difference observed between Θ_D^{HS} and Θ_D^{LS} shows that the intermolecular phonon spectrum sizably differs in the HS and LS phases, which provides evidence for the expected rearrangement of the crystal lattice upon the transition. This rearrangement seems to be rather moderate, owing to the low values of $\Delta\Theta_D/\Theta_D^{LS}$ (~11% for **1** and 9% for **2**), compared to those calculated from the Debye temperatures reported by König et al. for a number of iron(II) spin-crossover complexes (14–30%).[29-33]

A pronounced temperature dependence is observed for ΔE_q^{HS} (see Figure 10) whereas, as expected, ΔE_q^{LS} is almost independent of temperature (see Table VI). Concerning these data, some points have to be emphasized. (i) The magnitude of ΔE_q^{HS} values suggests that, for **1** and **2**, the high-spin ground state is an orbital singlet,[34] since orbital doublets usually lead to quadrupole splittings smaller than ~2 mm s^{-1}. This is consistent with the low symmetry of the coordination cores (nearly C_{2v}), which splits the $^5T_{2g}$ (O_h) term into three orbital singlets. (ii) It should be noted that the quasi-linearity of the curves above ~100 K is not consistent with a static ligand field approach.[35,36] In particular, a close similarity is observed between these curves and those reported for the high-spin Fe(II) ion in K_2ZnF_4, which have been interpreted by using a dynamic ligand field model.[37] (iii) A comparison of the slopes of the two ΔE_q^{HS} vs T curves, assimilated to straight lines, shows that the value obtained for **2** (~-4.1×10^{-3} mm s^{-1} K^{-1}), is lower than that determined for **1** (~4.6×10^{-3} mm s^{-1} K^{-1}). This indicates that the mean energy gap δ between the orbital ground state and the first two excited singlets, considered as being close to each other, is larger in **2** than in **1**. So, the distortion of the ligand field from octahedral symmetry is found to be higher in the former compound than in the latter. Since, in both cases, the bidentate ligands impart stronger ligand fields on the iron center than do the thiocyanate groups, this shows that, as expected, the ligand field strength of 1,10-phenanthroline is stronger than that of 2,2′-bipyrimidine. Assuming that the quoted slopes vary as δ^{-1}, a rough estimation of δ can be deduced from the data reported for $Fe^{II}(HS)$ in K_2ZnF_4 matrix[34] (slope of the ΔE_q vs T plot: ~-2.82×10^{-3} mm s^{-1} K^{-1}, δ = 590 cm^{-1}). For **1**, δ is found to lie in the range 300–400 cm^{-1}. For **2** it is about 10% larger.

Concerning the calorimetric data, it is worth noting that the peaks obtained for **1** are narrower than those relevant to **2**, which again emphasizes the higher cooperativity of the spin transition in the former compound, as demonstrated from the other experimental data (cf. Figures 4, 5, and 8).

The values found for the entropy variation (ΔS = 56 ± 4 (**1**) and 37 ± 5 J mol^{-1} K^{-1} (**2**)) are much greater than the contribution due to the spin multiplicity change alone, viz. $\Delta S_{spin} \simeq R \ln 5$ = 13.4 J mol^{-1} K^{-1}. The excess no doubt mainly arises from the changes in the vibrational characteristics of the coordination core and the lattice. Following Lord,[38] an order of magnitude of the lattice vibrational contribution, $\Delta S_{vib\,lat}$, has been evaluated by determining the thermodynamic functions of the crystal in the Debye approximation by means of tables from ref 39. For this, the Debye temperatures of the high- and low-spin phases have been assumed to be equal to those deduced from Mössbauer data (vide supra). It should be noted that the approximations used in this calculation are partly justified due to the relatively low values of transition temperatures. For **1**, the lattice vibrational entropies of the high- and low-spin forms, $S_{vib\,lat}$, were found to be 61.3 ± 1.5 and 55.9 ± 0.9 J mol^{-1} K^{-1}, respectively, leading to $\Delta S_{vib\,lat}$ = 5.4 ± 2.4 J mol^{-1} K^{-1}. For **2**, the following values were obtained: $(S_{vib\,lat})_{HS}$ = 53.7 ± 0.8 J mol^{-1} K^{-1}, $(S_{vib\,lat})_{LS}$ = 49.6 ± 1.0 J mol^{-1} K^{-1}; hence $\Delta S_{vib\,lat}$ = 4.1 ± 1.8 J mol^{-1} K^{-1}. So, for both compounds, $\Delta S_{vib\,lat}$ is shown to be very weak as compared with the total entropy variation. It follows that the main part of ΔS, estimated by difference to be ~51 J mol^{-1} K^{-1} for **1** and ~33 J mol^{-1} K^{-1} for **2**, has to be attributed to the intramolecular vibrational contribution $\Delta S_{vib\,mol}$ and, at least in the case of **1**, to the possible contribution of an order–disorder transition of the lattice pyridine.

Finally, let us consider the problem of the existence or the absence of a thermal hysteresis in the spin transitions exhibited by **1** and **2**. Concerning **2**, variable-temperature magnetic susceptibility measurements and Mössbauer scanning clearly show that such a hysteresis, if present, is too small to be observed from our experiments. On the other hand, in the case of **1**, hystereses of about 2.2, 3, and 7 K were measured from Mössbauer spectrometry, magnetism, and calorimetry experiments, respectively. There is no doubt that the observed discrepancy originates from the difference in the temperature scan rates, which are slightly lower than 0.1 K min^{-1} in the first technique, 0.5–1 K min^{-1} in the second one, and 10 K min^{-1} in the third one. From the evolution of the hysteresis values as a function of the scan rate, it clearly appears that the instrumental hysteresis resulting from the dynamic character of Mössbauer scan (the "slowest" technique) measurements should not exceed 0.1 K. So, evidence is provided for the existence of an intrinsic hysteresis of ~2 K for **1**.

Acknowledgment. We thank L. Toupet, Université de Rennes I, for X-ray data collections.

Supplementary Material Available: Full presentation of crystallographic data and experimental parameters for $Fe(py)_4(NCS)_2$ (Table SI) and $[Fe(py)_2bpym(NCS)_2]\cdot 0.25py$ (**1**) (Table SII), positional parameters for the non-hydrogen and hydrogen atoms of $Fe(py)_4(NCS)_2$ (Tables SIII and SIV, respectively) and **1** (Tables SV and SVI, respectively), anisotropic thermal parameters for $Fe(py)_4(NCS)_2$ (Table SVII) and **1** (Table SVIII), and distance and angle data associated with the heterocycles in $Fe(py)_4(NCS)_2$ (Table SIX) and **1** (Table SX) (10 pages); listings of calculated structure factors for $Fe(py)_4(NCS)_2$ and **1** (16 pages). Ordering information is given on any current masthead page.

(29) König, E.; Ritter, G.; Irler, W.; Goodwin, H. A. *J. Am. Chem. Soc.* **1980**, *102*, 4681.
(30) König, E.; Ritter, G.; Kulshreshtha, S. K.; Nelson, S. M. *Inorg. Chem.* **1982**, *21*, 3022.
(31) König, E.; Ritter, G.; Kulshreshtha, S. K.; Waigel, J.; Sacconi, L. *Inorg. Chem.* **1984**, *23*, 1241.
(32) König, E.; Ritter, G.; Kulshreshtha, S. A.; Waigel, J.; Goodwin, H. A. *Inorg. Chem.* **1984**, *23*, 1896.
(33) König, E.; Ritter, G.; Kulshreshtha, S. K.; Csatary, N. *Inorg. Chem.* **1984**, *23*, 1903.
(34) Varret, F. *J. Phys., Colloq.* **1976**, C6-437.
(35) Ingalls, R. *Phys. Rev.* **1964**, *133A*, 787.
(36) Price, D. C.; Varret, F. In *Advances in Mössbauer Spectroscopy*; Thosar, B. V., Srivastava, J. K., Iyengar, P. K., Bhargava, S. C., Eds.; Elsevier Scientific Publishing Co.: Amsterdam, Oxford, New York, 1983; p 316.
(37) Ducouret-Cérèze, A.; Varret, F. *J. Phys. (Paris)* **1988**, *49*, 661.
(38) Lord, R. C., Jr.; Ahlberg, J. E.; Andrews, D. H. *J. Chem. Phys.* **1938**, *5*, 649.
(39) Giguère, P. A.; Boisvert, M. *Tables des Fonctions Thermodynamiques de Debye*; Presses de l'Université Laval: Laval, Québec, 1962.